INTERNATIONAL JOURNAL FOR NUMERICAL METHODS IN ENGINEERING
Int. J. Numer. Meth. Engng 2017; **109**:1701–1720
Published online 2 September 2016 in Wiley Online Library (wileyonlinelibrary.com). DOI: 10.1002/nme.5349

A dynamic condensation method using algebraic substructuring

Seung-Hwan Boo and Phill-Seung Lee*,†

Department of Mechanical Engineering, Korea Advanced Institute of Science and Technology, 291 Daehak-ro, Yuseong-gu, Daejeon 34141, Korea

SUMMARY

In this paper, we develop a robust reduced-order modeling method, named algebraic dynamic condensation, which is based on the improved reduced system method. Using algebraic substructuring, the global mass and stiffness matrices are divided into many small submatrices without considering the physical domain, and substructures and interface boundary are defined in the algebraic perspective. The reduced model is then constructed using three additional procedures: substructural stiffness condensation, interface boundary reduction, and substructural inertial effect condensation. The formulation of the reduced model is simply expressed at a submatrix level without using a transformation matrix that induces huge computational cost. Through various numerical examples, the performance of the proposed method is demonstrated in terms of accuracy and computational cost. Copyright © 2016 John Wiley & Sons, Ltd.

Received 6 February 2016; Accepted 4 August 2016

KEY WORDS: structural dynamics; finite element method; reduced-order modeling; algebraic substructuring; Eigenvalue problem

1. INTRODUCTION

In structural dynamics, dynamic condensation methods [1–15] have been widely used for decades to reduce the degrees of freedom (DOFs) of a large finite element (FE) model. In dynamic condensation methods, DOFs in the original FE model are separated into the retained and truncated DOFs, and the reduced model is constructed by condensing the stiffness and inertial effects for the truncated DOFs into retained DOFs. Dynamic condensation methods have been employed in various engineering fields such as structural health monitoring, FE model updating, experimental modal analysis and experimental-FE model correlation [1–11].

In the 1960s, Guyan [1] and Irons [2] independently proposed a static condensation method. Because, in the static condensation, the inertia effects of the truncated DOFs are ignored, the solution accuracy for higher modes is not good. In 1989, considering the inertia effects properly, O'Callahan [7] proposed the improved reduced system (IRS) method. The IRS method has been widely adopted because of its excellent solution accuracy and simple formulation. Since then, Friswell [10] developed the iterative IRS method (IIRS), and Xia and Lin [11] improved the IIRS method. While the IIRS method can provide further improved accuracy, additional computational cost is inevitable. In order to improve computational efficiency, Bouhaddi and Fillod [12–14] applied physical domain-based substructuring, which is a key concept of component mode synthesis (CMS) methods [16–23], to the Guyan reduction. Kim and Cho [24, 25] applied physical domain-based substructuring to the IRS and IIRS methods.

Since the 1970s, several algebraic substructuring algorithms have been developed in applied mathematics [26–29]. In algebraic substructuring, a large sparse matrix is automatically divided into

*Correspondence to: Phill-Seung Lee, Department of Mechanical Engineering, Korea Advanced Institute of Science and Technology, 291 Daehak-ro, Yuseong-gu, Daejeon 34141, Korea.
†E-mail: phillseung@kaist.edu

many small submatrices without consideration of the physical domain. Therefore, a large number of substructures (submatrices) can be effectively managed in computation, and thus, computational cost can be significantly reduced. Algebraic substructuring was successfully applied to the CMS methods [30–34], and it offered remarkable computational efficiency.

In this study, we develop a new efficient reduced-order modeling technique, named algebraic dynamic condensation. The formulation is based on the IRS method. The design focus is on computational efficiency, which is achieved avoiding expensive global matrix operations and matrix populations. First, global mass and stiffness matrices are automatically partitioned using algebraic substructuring. The substructural stiffness is then condensed into the interface boundary, and the interface boundary is reduced considering the dominant interface normal modes. Finally, the reduced model is constructed by condensing the substructural inertial effects into the reduced interface boundary.

The formulation of the proposed method can be simply expressed using multiplications and summations of submatrices, and thus, it presents excellent computational efficiency in comparison to the IRS method. The proposed method also provides better accuracy than the IRS method. A great feature of our method is that, as the number of substructures (submatrices) increases, both accuracy and computation cost improve, and unlike the IRS method, the proposed method can handle relatively large FE models. We also investigate the performance of the proposed method compared with the Craig–Bampton (CB) method, which is a well-known and widely used CMS method.

In Section 2, the formulation of the IRS method is briefly reviewed, and the proposed method is formulated in Section 3. Using several structural problems, the performance of our method is demonstrated and compared with the IRS and CB methods in Sections 4 and 5, respectively. Finally, conclusions are drawn in Section 6.

2. IMPROVED REDUCED SYSTEM METHOD

In this section, we briefly review the formulation of the IRS method for a structural FE model. The detailed derivations are well presented in References [7–10].

In the IRS method, the equations of motion for free vibration without damping are given by

$$\mathbf{M}_g \ddot{\mathbf{u}}_g + \mathbf{K}_g \mathbf{u}_g = \mathbf{0}, \tag{1}$$

$$\text{with } \mathbf{M}_g = \begin{bmatrix} \mathbf{M}_t & \mathbf{M}_{tr} \\ \mathbf{M}_{tr}^T & \mathbf{M}_r \end{bmatrix}, \mathbf{K}_g = \begin{bmatrix} \mathbf{K}_t & \mathbf{K}_{tr} \\ \mathbf{K}_{tr}^T & \mathbf{K}_r \end{bmatrix}, \mathbf{u}_g = \begin{bmatrix} \mathbf{u}_t \\ \mathbf{u}_r \end{bmatrix}, \tag{2}$$

where $\mathbf{M}_g$ and $\mathbf{K}_g$ are the global mass and stiffness matrices, respectively, $\mathbf{u}_g$ is the global displacement vector, and $(\ddot{}) = d^2(\ )/dt^2$ represents second-order differentiation with respect to the time variable. The subscripts t and r denote the truncated and retained DOFs, respectively, while the subscript tr denotes the coupled DOFs between the truncated and retained DOFs.

The eigenvalue problem for the global structural FE model is given by

$$\mathbf{K}_g(\boldsymbol{\varphi}_g)_i = \lambda_i \mathbf{M}_g(\boldsymbol{\varphi}_g)_i \text{ for } i = 1, 2, \ldots, N_g, \tag{3}$$

and, using the calculated eigenvectors, the global displacement vector $\mathbf{u}_g$ is expressed by

$$\mathbf{u}_g = \boldsymbol{\Phi}_g \mathbf{q}_g \tag{4a}$$

$$\text{with } \boldsymbol{\Phi}_g = [\,(\boldsymbol{\varphi}_g)_1\ (\boldsymbol{\varphi}_g)_2 \cdots (\boldsymbol{\varphi}_g)_{N_g}\,], \mathbf{q}_g = \begin{bmatrix} \mathbf{q}_1 \\ \mathbf{q}_2 \\ \vdots \\ \mathbf{q}_{N_g} \end{bmatrix}, \tag{4b}$$

in which λ_i and $(\boldsymbol{\varphi}_g)_i$ are the eigenvalue and eigenvector corresponding to the ith global mode, and N_g is the number of DOFs in the global FE model. Here, $\boldsymbol{\Phi}_g$ is the global eigenvector matrix that

DOI: 10.1002/nme

contains the eigenvectors $(\boldsymbol{\varphi}_g)_i$, and $\mathbf{q}_g$ is the generalized coordinate vector. Note that $(\boldsymbol{\varphi}_g)_i$ is the mass-normalized eigenvector.

Using the relation $(\ddot{\ }) = d^2(\ )/dt^2 = -\lambda(\ )$, Equation (1) is rewritten as

$$\begin{bmatrix} \mathbf{K}_t & \mathbf{K}_{tr} \\ \mathbf{K}_{tr}^T & \mathbf{K}_r \end{bmatrix} \begin{bmatrix} \mathbf{u}_t \\ \mathbf{u}_r \end{bmatrix} = \lambda \begin{bmatrix} \mathbf{M}_t & \mathbf{M}_{tr} \\ \mathbf{M}_{tr}^T & \mathbf{M}_r \end{bmatrix} \begin{bmatrix} \mathbf{u}_t \\ \mathbf{u}_r \end{bmatrix}, \tag{5}$$

and, expanding the first row equation, the truncated DOF vector $\mathbf{u}_t$ is represented by

$$\begin{aligned} \mathbf{u}_t &= -(\mathbf{K}_t - \lambda\,\mathbf{M}_t)^{-1}(\mathbf{K}_{tr} - \lambda\,\mathbf{M}_{tr})\mathbf{u}_r \\ &= [-\mathbf{K}_t^{-1}\mathbf{K}_{tr} + \lambda\mathbf{K}_t^{-1}\,(\mathbf{M}_{tr} - \mathbf{M}_t\mathbf{K}_t^{-1}\mathbf{K}_{tr}) + o(\lambda^2) + o(\lambda^3) + \cdots]\ \mathbf{u}_r. \end{aligned} \tag{6}$$

Neglecting higher order terms of λ in Equation (6), the truncated DOF vector is approximated as

$$\mathbf{u}_t \approx \bar{\mathbf{u}}_t = [-\mathbf{K}_t^{-1}\mathbf{K}_{tr}\ + \lambda\,\mathbf{K}_t^{-1}\,(\mathbf{M}_{tr} - \mathbf{M}_t\mathbf{K}_t^{-1}\mathbf{K}_{tr})]\ \mathbf{u}_r, \tag{7}$$

and then the global displacement vector $\mathbf{u}_g$ is approximated as

$$\mathbf{u}_g \approx\ \bar{\mathbf{u}}_g = \begin{bmatrix} \bar{\mathbf{u}}_t \\ \mathbf{u}_r \end{bmatrix} = (\mathbf{T}_G + \lambda\,\mathbf{T}_a)\mathbf{u}_r, \tag{8a}$$

$$\text{with } \mathbf{T}_G = \begin{bmatrix} -\mathbf{K}_t^{-1}\mathbf{K}_{tr} \\ \mathbf{I}_r \end{bmatrix}, \mathbf{T}_a = \begin{bmatrix} \mathbf{K}_t^{-1}\,(\mathbf{M}_{tr} - \mathbf{M}_t\mathbf{K}_t^{-1}\mathbf{K}_{tr}) \\ \mathbf{0} \end{bmatrix}, \tag{8b}$$

in which $\mathbf{T}_G$ denotes the Guyan transformation matrix [1] called the 'static condensation matrix', $\mathbf{T}_a$ is an additional transformation matrix containing the inertial effects of the truncated DOFs, and $\mathbf{I}_r$ is the identity matrix for the retained DOFs. The overbar ($\bar{\ }$) denotes the approximated quantities.

Considering only the transformation matrix $\mathbf{T}_G$ in Equation (8a), the approximated global displacement vector $\bar{\mathbf{u}}_g$ in the Guyan reduction is defined by

$$\bar{\mathbf{u}}_g = \mathbf{T}_G\mathbf{u}_r, \tag{9}$$

and the resulting reduced eigenvalue problem becomes

$$\overline{\mathbf{K}}_G\,\mathbf{u}_r = \bar{\lambda}\,\overline{\mathbf{M}}_G\mathbf{u}_r \text{ with } \overline{\mathbf{M}}_G = \mathbf{T}_G^T\mathbf{M}_g\mathbf{T}_G, \overline{\mathbf{K}}_G = \mathbf{T}_G^T\mathbf{K}_g\mathbf{T}_G, \tag{10}$$

where $\overline{\mathbf{M}}_G$ and $\overline{\mathbf{K}}_G$ are the reduced mass and stiffness matrices in the Guyan reduction, and $\bar{\lambda}$ is the approximated eigenvalue.

The matrix $\overline{\mathbf{M}}_G^{-1}$ is pre-multiplied on the left-hand and right-hand sides of Equation (10), and the following equation is obtained

$$\bar{\lambda}\,\mathbf{u}_r = \mathbf{H}_G\mathbf{u}_r \text{ with } \mathbf{H}_G = \overline{\mathbf{M}}_G^{-1}\overline{\mathbf{K}}_G. \tag{11}$$

Substituting Equation (11) into Equation (8a), the approximated global displacement vector $\bar{\mathbf{u}}_g$ is redefined as

$$\bar{\mathbf{u}}_g = \mathbf{T}_1\mathbf{u}_r \text{ with } \mathbf{T}_1 = \mathbf{T}_G + \mathbf{T}_a\mathbf{H}_G, \tag{12}$$

in which $\mathbf{T}_1$ is the transformation matrix of the IRS (improved reduced system) method.

The reduced mass and stiffness matrices in the IRS method are obtained as

$$\overline{\mathbf{M}}_1 = \mathbf{T}_1^T\mathbf{M}_g\mathbf{T}_1 = \overline{\mathbf{M}}_G + \mathbf{T}_G^T\mathbf{M}_g\mathbf{T}_a\mathbf{H}_G + \mathbf{H}_G^T\mathbf{T}_a^T\mathbf{M}_g\mathbf{T}_G + \mathbf{H}_G^T\mathbf{T}_a^T\mathbf{M}_g\mathbf{T}_a\mathbf{H}_G, \tag{13a}$$

$$\overline{\mathbf{K}}_1 = \mathbf{T}_1^T\mathbf{K}_g\mathbf{T}_1 = \overline{\mathbf{K}}_G + \mathbf{T}_G^T\mathbf{K}_g\mathbf{T}_a\mathbf{H}_G + \mathbf{H}_G^T\mathbf{T}_a^T\mathbf{K}_g\mathbf{T}_G + \mathbf{H}_G^T\mathbf{T}_a^T\mathbf{K}_g\mathbf{T}_a\mathbf{H}_G. \tag{13b}$$

The reduced eigenvalue problem is given by

$$\overline{\mathbf{K}}_1(\bar{\boldsymbol{\varphi}})_i = \bar{\lambda}_i\,\overline{\mathbf{M}}_1\,(\bar{\boldsymbol{\varphi}})_i \text{for } i = 1, 2, \ldots, \overline{N}, \tag{14}$$

DOI: 10.1002/nme

where $\bar{\lambda}_i$ and $(\bar{\boldsymbol{\varphi}})_i$ are the approximated eigenvalues and eigenvectors in the IRS method, $\overline{N}$ is the number of DOFs in the reduced model ($\overline{N} = N_r$, in which N_r is the number of the retained DOFs), and the approximated global eigenvector $(\bar{\boldsymbol{\varphi}})_i$ can be calculated by

$$(\bar{\boldsymbol{\varphi}}_g)_i = \mathbf{T}_1 \bar{\boldsymbol{\varphi}}_i. \tag{15}$$

The transformation procedure in Equation (13) is performed through simple matrix multiplications. However, because the matrices in Equation (13) are the size of the global system (N_g) and the transformation matrices are highly populated, the required computational cost could be huge for large FE models.

3. ALGEBRAIC DYNAMIC CONDENSATION METHOD

In this section, we describe the key procedures of the algebraic dynamic condensation method: algebraic substructuring, substructural stiffness condensation, interface boundary reduction, and substructural inertial effect condensation.

The design focus of the proposed method is on computational efficiency and thus expensive global matrix operations and matrix populations are avoided within the formulation.

3.1. Algebraic substructuring

In algebraic substructuring, rows and columns of an original large sparse matrix are permuted, and the permuted matrix is then partitioned into many submatrices; see Figure 1. Note that the matrix permutation is performed by renumbering nodes in FE models. The permutation procedure does not alter the physical characteristic of original FE models.

In a large FE model, the original mass and stiffness matrices are large and sparse. Using the algebraic substructuring procedure, the matrices can be automatically partitioned into many submatrices. Here, those submatrices could be defined as substructures and the interface boundary in the algebraic perspective.

After the algebraic substructuring, the global mass and stiffness matrices, $\mathbf{M}_g$ and $\mathbf{K}_g$, are partitioned into n substructures and the interface boundary

$$\mathbf{M}_g = \left[\begin{array}{ccc:c} \mathbf{M}_1 & & \mathbf{0} & \mathbf{M}_1^c \\ & \ddots & & \vdots \\ \mathbf{0} & & \mathbf{M}_n & \mathbf{M}_n^c \\ \hdashline (\mathbf{M}_1^c)^T & \cdots & (\mathbf{M}_n^c)^T & \mathbf{M}_b \end{array}\right], \quad \mathbf{K}_g = \left[\begin{array}{ccc:c} \mathbf{K}_1 & & \mathbf{0} & \mathbf{K}_1^c \\ & \ddots & & \vdots \\ \mathbf{0} & & \mathbf{K}_n & \mathbf{K}_n^c \\ \hdashline (\mathbf{K}_1^c)^T & \cdots & (\mathbf{K}_n^c)^T & \mathbf{K}_b \end{array}\right], \tag{16}$$

in which $\mathbf{M}_i$ and $\mathbf{K}_i$ denote the diagonal component mass and stiffness matrices of the ith substructure, respectively, and $\mathbf{M}_b$ and $\mathbf{K}_b$ denote the mass and stiffness matrices of the interface boundary, respectively. The off-diagonal component matrices $\mathbf{M}_i^c$ and $\mathbf{K}_i^c$ denote the mass and stiffness matrices of the ith substructure coupled with the interface boundary. Note that the global partitioned matrices in Equation (16) have the same form as used in the CB method [17].

3.2. Substructural stiffness condensation

Using the partitioned mass and stiffness matrices in Equation (16), the eigenvalue problem for the global structure is expressed as

$$\begin{bmatrix} \mathbf{K}_s & \mathbf{K}_c \\ \mathbf{K}_c^T & \mathbf{K}_b \end{bmatrix} \begin{bmatrix} \mathbf{u}_s \\ \mathbf{u}_b \end{bmatrix} = \lambda \begin{bmatrix} \mathbf{M}_s & \mathbf{M}_c \\ \mathbf{M}_c^T & \mathbf{M}_b \end{bmatrix} \begin{bmatrix} \mathbf{u}_s \\ \mathbf{u}_b \end{bmatrix}, \tag{17}$$

where the subscripts s and b denote the substructural and interface boundary quantities, respectively, and the subscript c denotes the coupled quantities between the substructures and interface boundary.

DOI: 10.1002/nme

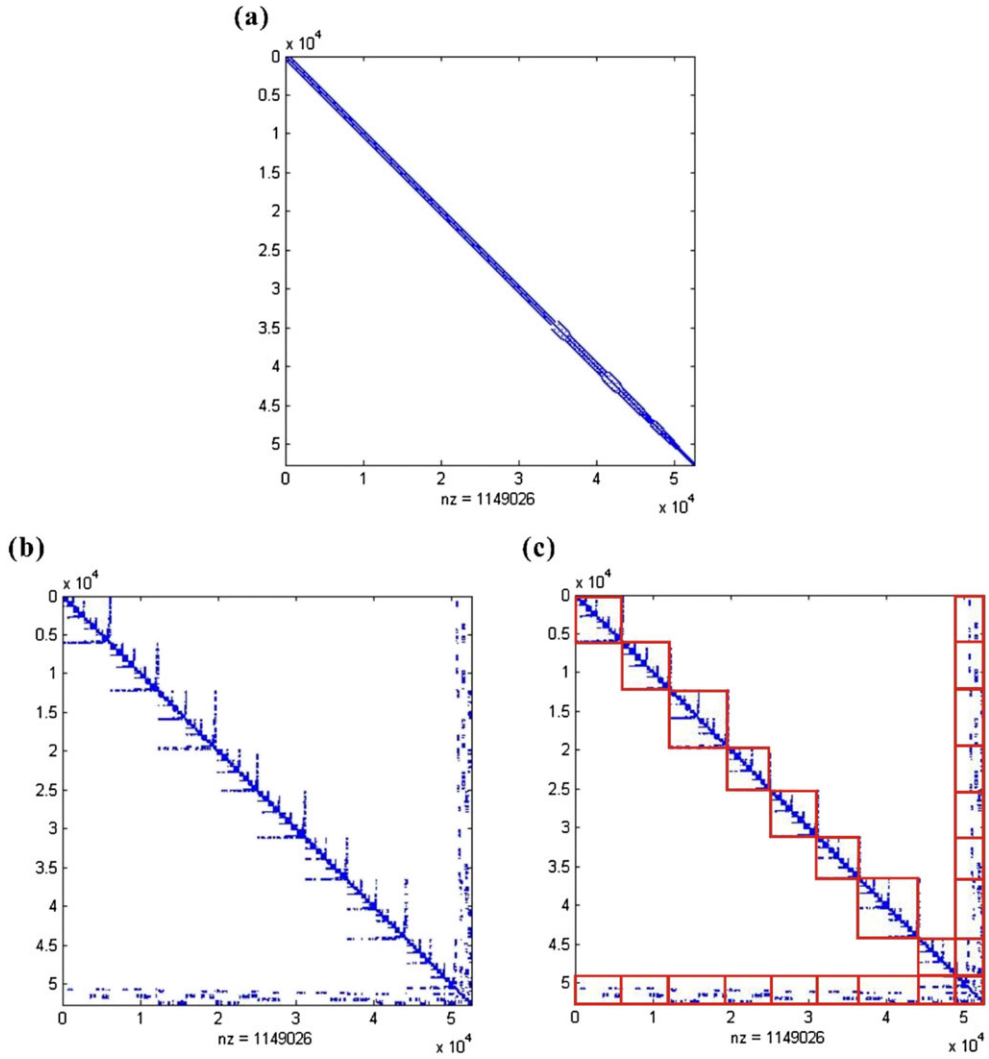

Figure 1. Algebraic substructuring procedure: (a) Nonzero pattern of an original large sparse matrix, (b) Nonzero pattern of the permuted matrix, (c) Matrix substructuring (eight substructures and the interface boundary).

$\mathbf{M}_s$ and $\mathbf{K}_s$ are the block-diagonal mass and stiffness matrices that consist of the substructural mass and stiffness matrices, $\mathbf{M}_i$ and $\mathbf{K}_i$.

From the first row in Equation (17), the substructural displacement vector $\mathbf{u}_s$ is represented in terms of $\mathbf{u}_b$

$$\mathbf{u}_s = -(\mathbf{K}_s - \lambda\,\mathbf{M}_s)^{-1}(\mathbf{K}_c - \lambda\,\mathbf{M}_c)\mathbf{u}_b = [\boldsymbol{\Psi}_c + \lambda\,\mathbf{K}_s^{-1}\,\hat{\mathbf{M}}_c + o(\lambda^2) + o(\lambda^3) + \cdots]\,\mathbf{u}_b, \quad (18a)$$

$$\text{with } \boldsymbol{\Psi}_c = -\mathbf{K}_s^{-1}\mathbf{K}_c, \hat{\mathbf{M}}_c = \mathbf{M}_c + \mathbf{M}_s\boldsymbol{\Psi}_c, \quad (18b)$$

in which the global eigenvalue λ is an unknown scalar value. Neglecting terms with λ in Equation (18a), the substructural displacement vector $\mathbf{u}_s$ can be approximated by the interface displacement vector $\mathbf{u}_b$

$$\mathbf{u}_s \approx \bar{\mathbf{u}}_s = \boldsymbol{\Psi}_c\mathbf{u}_b, \quad (19)$$

and, then the global displacement vector $\mathbf{u}_g$ is approximated by

$$\mathbf{u}_g \approx \bar{\mathbf{u}}_g = \begin{bmatrix} \bar{\mathbf{u}}_s \\ \mathbf{u}_b \end{bmatrix} = \boldsymbol{\Psi}\,\mathbf{u}_b \text{ with } \boldsymbol{\Psi} = \begin{bmatrix} \boldsymbol{\Psi}_c \\ \mathbf{I}_b \end{bmatrix}, \quad (20)$$

DOI: 10.1002/nme

where $\boldsymbol{\Psi}$ denotes the interface constraint mode matrix [17], $\boldsymbol{\Psi}_c$ is the constraint mode matrix to couple the substructures with the interface boundary, and $\mathbf{I}_b$ is the identity matrix for the interface boundary. Note that $\boldsymbol{\Psi}$ is identical to the Guyan transformation matrix $\mathbf{T}_G$ in Equation (8b). That is, $\boldsymbol{\Psi}$ is the static condensation matrix that condenses the substructural stiffness into the interface boundary.

The submatrix form of $\boldsymbol{\Psi}$ in Equation (20) is described as

$$\boldsymbol{\Psi} = \begin{bmatrix} \boldsymbol{\Psi}_1^c \\ \boldsymbol{\Psi}_2^c \\ \vdots \\ \boldsymbol{\Psi}_n^c \\ \mathbf{I}_b \end{bmatrix} \text{ with } \boldsymbol{\Psi}_i^c = -(\mathbf{K}_i^s)^{-1}\mathbf{K}_i^c \text{ for } i = 1, 2, \ldots, n, \tag{21}$$

where $\boldsymbol{\Psi}_i^c$ is the constraint mode matrix to couple the ith substructure with the interface boundary. Here, the inverse matrix $(\mathbf{K}_i^s)^{-1}$ can be effectively computed using the Cholesky factorization of $\mathbf{K}_i^s$. Substituting Equation (20) into Equation (17) and pre-multiplying $\boldsymbol{\Psi}^T$, the following reduced eigenvalue problem is obtained

$$\hat{\mathbf{K}}_b\mathbf{u}_b = \bar{\lambda}\hat{\mathbf{M}}_b\mathbf{u}_b, \tag{22}$$

with

$$\hat{\mathbf{M}}_b = \boldsymbol{\Psi}^T\mathbf{M}_g\boldsymbol{\Psi} = \mathbf{M}_b + \mathbf{M}_c^T\boldsymbol{\Psi}_c + \boldsymbol{\Psi}_c^T\hat{\mathbf{M}}_c, \tag{23a}$$

$$\hat{\mathbf{K}}_b = \boldsymbol{\Psi}^T\mathbf{K}_g\boldsymbol{\Psi} = \mathbf{K}_b + \mathbf{K}_c^T\boldsymbol{\Psi}_c, \tag{23b}$$

in which $\hat{\mathbf{M}}_b$ and $\hat{\mathbf{K}}_b$ are the reduced mass and stiffness matrices of size $N_b \times N_b$ (N_b is the number of DOFs in the interface boundary).

The matrices $\mathbf{M}_c$, $\boldsymbol{\Psi}_c$, $\hat{\mathbf{M}}_c$, and $\mathbf{K}_c$ in Equation (23) are represented in submatrix form as

$$\mathbf{M}_c = \begin{bmatrix} \mathbf{M}_1^c \\ \mathbf{M}_2^c \\ \vdots \\ \mathbf{M}_n^c \end{bmatrix}, \quad \boldsymbol{\Psi}_c = \begin{bmatrix} \boldsymbol{\Psi}_1^c \\ \boldsymbol{\Psi}_2^c \\ \vdots \\ \boldsymbol{\Psi}_n^c \end{bmatrix}, \quad \hat{\mathbf{M}}_c = \begin{bmatrix} \hat{\mathbf{M}}_1^c \\ \hat{\mathbf{M}}_2^c \\ \vdots \\ \hat{\mathbf{M}}_n^c \end{bmatrix}, \quad \mathbf{K}_c = \begin{bmatrix} \mathbf{K}_1^c \\ \mathbf{K}_2^c \\ \vdots \\ \mathbf{K}_n^c \end{bmatrix}, \tag{24}$$

and then the reduced mass and stiffness matrices can be effectively calculated at the submatrix level through the following submatrix operations

$$\hat{\mathbf{M}}_b = \mathbf{M}_b + \sum_{i=1}^{n}(\mathbf{M}_i^c)^T\boldsymbol{\Psi}_i^c + \sum_{i=1}^{n}(\boldsymbol{\Psi}_i^c)^T\hat{\mathbf{M}}_i^c \text{ with } \hat{\mathbf{M}}_i^c = \mathbf{M}_i^c + \mathbf{M}_i\boldsymbol{\Psi}_i^c, \tag{25a}$$

Table I. Computational procedure of the algebraic dynamic condensation.

Computational procedure	Related equations
Step 1. Algebraic substructuring of $\mathbf{M}_g$ and $\mathbf{K}_g$	16
Step 2. Substructural stiffness condensation	
a. Compute $-(\mathbf{K}_i^s)^{-1}$, $\boldsymbol{\Psi}_i^c$ and $\hat{\mathbf{M}}_i^c$.	21, 25a
b. Calculate $\hat{\mathbf{M}}_b$ and $\hat{\mathbf{K}}_b$.	25
Step 3. Interface boundary reduction	
a. Calculate the dominant interface normal mode matrix, $\boldsymbol{\Phi}_b^d$	27
b. Calculate $\overline{\mathbf{M}}_b$ and $\overline{\mathbf{K}}_b$.	29
Step 4. Substructural inertial effect condensation	
a. Calculate $\mathbf{H}_b$, $\mathbf{A}_i$, $\mathbf{R}_1$ and $\mathbf{R}_2$.	34, 37, 38b
b. Calculate the reduced matrices, $\tilde{\mathbf{M}}_b$ and $\tilde{\mathbf{K}}_b$.	38a

DOI: 10.1002/nme

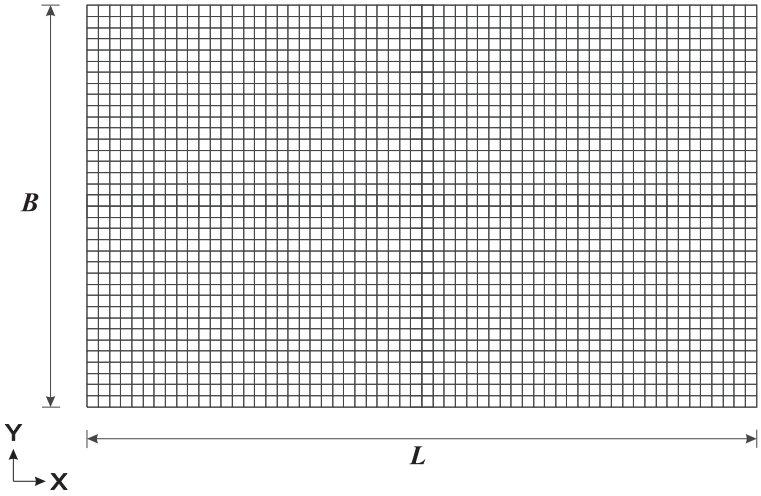

Figure 2. Rectangular plate problem (60 × 36 mesh, 11,285 DOFs).

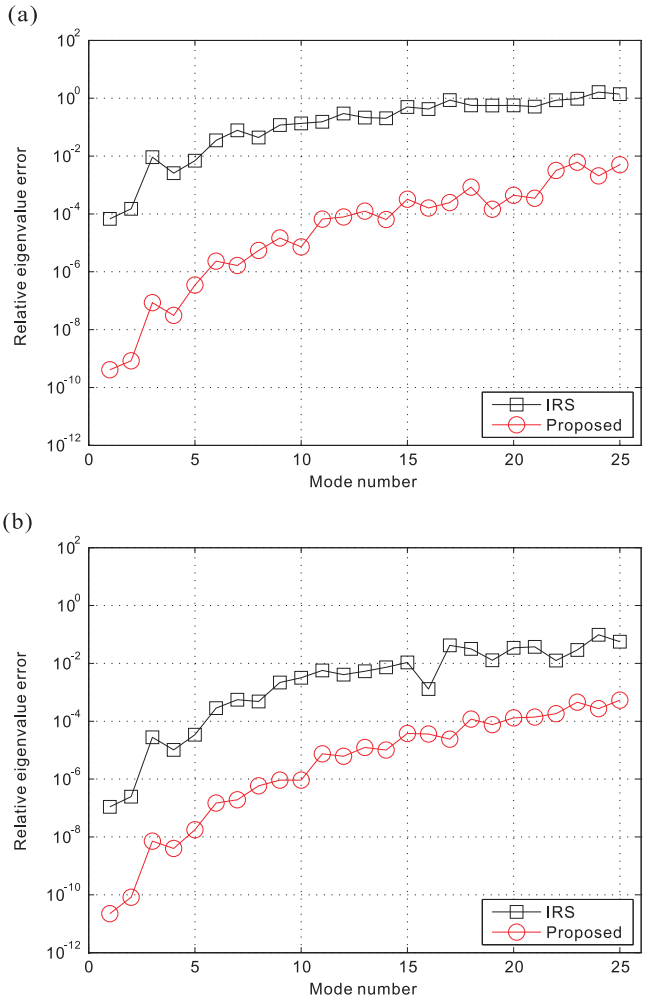

Figure 3. Relative eigenvalue errors by the IRS and proposed methods for the rectangular plate problem: (a) $N_r = 100$ and $\overline{N}_b = 100$ (b) $N_r = 300$ and $\overline{N}_b = 300$.

DOI: 10.1002/nme

$$\hat{\mathbf{K}}_b = \mathbf{K}_b + \sum_{i=1}^{n} (\mathbf{K}_i^c)^T \boldsymbol{\Psi}_i^c. \tag{25b}$$

3.3. Interface boundary reduction

As the number of substructures increases, the DOFs of the interface boundary rapidly grows. In order to avoid the escalating computational cost, it is essential to reduce the interface boundary.

After solving the reduced eigenvalue problem in Equation (22), the interface displacement vector $\mathbf{u}_b$ can be expressed as

$$\mathbf{u}_b = \boldsymbol{\Phi}_b \, \mathbf{q}_b, \tag{26}$$

in which $\boldsymbol{\Phi}_b$ is the interface eigenvector matrix, and $\mathbf{q}_b$ is the corresponding generalized coordinate vector.

Table II. Relative eigenvalue errors for the rectangular plate problem when $N_r = \overline{N}_b = 100$.

Mode number	IRS	Proposed
1	6.76228E-05	4.10733E-10
2	1.49447E-04	8.54147E-10
3	9.19271E-03	8.54488E-08
4	2.56983E-03	3.11311E-08
5	6.90573E-03	3.50102E-07
6	3.50973E-02	2.33387E-06
7	7.79645E-02	1.64861E-06
8	4.39716E-02	5.49240E-06
9	1.18145E-01	1.47466E-05
10	1.34452E-01	7.27208E-06
11	1.53947E-01	6.60347E-05
12	2.96908E-01	7.86423E-05
13	2.15174E-01	1.24925E-04
14	2.02588E-01	6.41646E-05
15	4.96222E-01	3.22909E-04
16	4.24919E-01	1.60237E-04
17	8.63934E-01	2.46142E-04
18	5.63174E-01	8.42677E-04
19	5.58491E-01	1.45123E-04
20	5.65632E-01	4.43949E-04
21	5.14183E-01	3.48023E-04
22	8.48793E-01	3.16917E-03
23	9.60316E-01	6.11854E-03
24	1.62232E+00	2.06494E-03
25	1.39140E+00	5.03076E-03

Table III. Specific computational cost for the rectangular plate problem when $N_r = \overline{N}_b = 100$.

Methods	Items	Related Equations	Computation times [sec]	Computation times Ratio [%]
IRS	Transformation procedure	8, 13	205.70	99.95
	Reduced eigenvalue problem	14	0.10	0.05
	Total	—	205.80	100.00
Proposed	Algebraic substructuring	16	0.05	0.02
	Calculation of $\hat{\mathbf{M}}_b$ and $\hat{\mathbf{K}}_b$ matrices	25	0.61	0.30
	Eigenvalue problem for the interface boundary	26	0.49	0.24
	Calculation of $\overline{\mathbf{M}}_b$, $\overline{\mathbf{K}}_b$ and $\mathbf{H}_b$ matrices	29, 34	0.03	0.01
	Calculation of $\tilde{\mathbf{M}}_b$ and $\tilde{\mathbf{K}}_b$ matrices	38	0.70	0.34
	Reduced eigenvalue problem	39	0.10	0.05
	Total	—	1.98	0.96

DOI: 10.1002/nme

In Equation (26), $\mathbf{\Phi}_b$ and $\mathbf{q}_b$ can be decomposed into the dominant and residual terms as follows

$$\mathbf{\Phi}_b = [\mathbf{\Phi}_b^d \;\; \mathbf{\Phi}_b^r], \quad \mathbf{q}_b = \begin{bmatrix} \mathbf{q}_b^d \\ \mathbf{q}_b^r \end{bmatrix} \tag{27}$$

where $\mathbf{\Phi}_b^d$ and $\mathbf{\Phi}_b^r$ are the dominant and residual interface normal modes, respectively, and $\mathbf{q}_b^d$ and $\mathbf{q}_b^r$ are the generalized coordinate vectors corresponding to $\mathbf{\Phi}_b^d$ and $\mathbf{\Phi}_b^r$, respectively.

Considering only the dominant interface normal modes $\mathbf{\Phi}_b^d$, we can obtain the reduced interface displacement vector $\bar{\mathbf{u}}_b$ as

$$\mathbf{u}_b \approx \bar{\mathbf{u}}_b = \mathbf{\Phi}_b^d \, \mathbf{q}_b^d, \tag{28}$$

in which $\mathbf{\Phi}_b^d$ can be effectively calculated by using the shift-invert Lanczos algorithm.

Using Equation (28) in Equation (22), the eigenvalue problem for the reduced interface boundary is obtained as

$$\overline{\mathbf{K}}_b \, \mathbf{q}_b^d = \bar{\lambda} \, \overline{\mathbf{M}}_b \, \mathbf{q}_b^d \text{ with } \overline{\mathbf{M}}_b = (\mathbf{\Phi}_b^d)^T \hat{\mathbf{M}}_b \, (\mathbf{\Phi}_b^d), \overline{\mathbf{K}}_b = (\mathbf{\Phi}_b^d)^T \hat{\mathbf{K}}_b \, (\mathbf{\Phi}_b^d), \tag{29}$$

in which $\overline{\mathbf{M}}_b$ and $\overline{\mathbf{K}}_b$ are the mass and stiffness matrices for the reduced interface boundary, and $\bar{\lambda}$ is the approximated eigenvalue. Note that $\overline{\mathbf{M}}_b$ and $\overline{\mathbf{K}}_b$ are $\overline{N}_b \times \overline{N}_b$ matrices, where $\overline{N}_b$ is the number of the dominant interface normal modes.

3.4. Substructural inertial effect condensation

Considering the first order term of λ in Equation (18a), the approximated substructural displacement vector $\bar{\mathbf{u}}_s$ in Equation (19) becomes more precise

$$\bar{\mathbf{u}}_s = (\mathbf{\Psi}_c + \lambda \, \mathbf{K}_s^{-1} \, \hat{\mathbf{M}}_c)\mathbf{u}_b. \tag{30}$$

Combining Equations (28) and (30), the approximated global displacement vector $\bar{\mathbf{u}}_g$ in Equation (20) is redefined as

$$\bar{\mathbf{u}}_g = \begin{bmatrix} \bar{\mathbf{u}}_s \\ \bar{\mathbf{u}}_b \end{bmatrix} = \mathbf{\Psi}_1 \mathbf{q}_b^d \text{ with } \mathbf{\Psi}_1 = \bar{\mathbf{\Psi}} + \lambda \, \mathbf{\Psi}_a, \bar{\mathbf{\Psi}} = \begin{bmatrix} \mathbf{\Psi}_c \mathbf{\Phi}_b^d \\ \mathbf{\Phi}_b^d \end{bmatrix}, \mathbf{\Psi}_a = \begin{bmatrix} \mathbf{K}_s^{-1} \hat{\mathbf{M}}_c \mathbf{\Phi}_b^d \\ \mathbf{0} \end{bmatrix}, \tag{31}$$

where $\mathbf{\Psi}_1$ is a newly defined interface constraint mode matrix compensating for the inertial effects of the substructures by $\lambda \mathbf{\Psi}_a$, and $\bar{\mathbf{\Psi}}$ is the reduced interface constraint mode matrix.

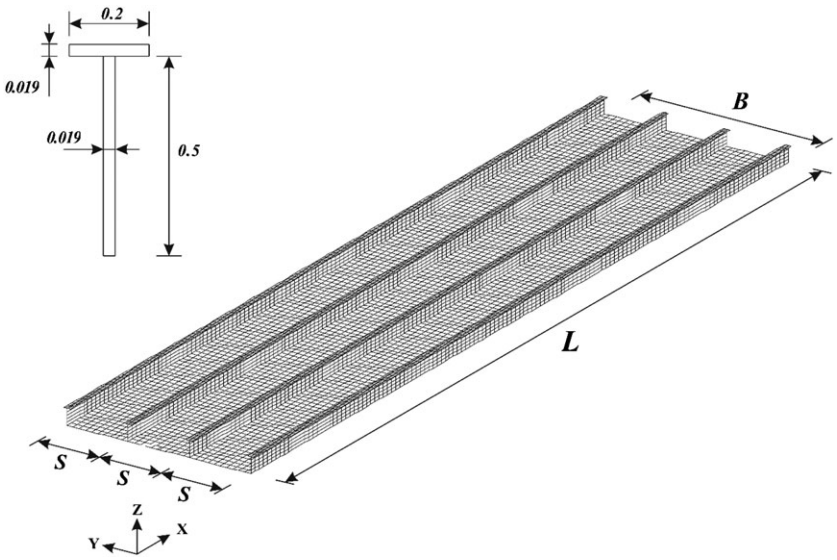

Figure 4. Stiffened plate problem (8,580 shell elements, 52,662 DOFs).

DOI: 10.1002/nme

Employing the matrix $\boldsymbol{\Psi}_1$ in Equation (31), the following reduced matrices are defined as

$$\tilde{\mathbf{M}}_b = \boldsymbol{\Psi}_1^T \mathbf{M}_g \boldsymbol{\Psi}_1 = \overline{\mathbf{M}}_b + \lambda\, \bar{\boldsymbol{\Psi}}^T \mathbf{M}_g \boldsymbol{\Psi}_a + \lambda\, \boldsymbol{\Psi}_a^T \mathbf{M}_g \bar{\boldsymbol{\Psi}} + \lambda^2 \boldsymbol{\Psi}_a^T \mathbf{M}_g \boldsymbol{\Psi}_a, \tag{32a}$$

$$\tilde{\mathbf{K}}_b = \boldsymbol{\Psi}_1^T \mathbf{K}_g \boldsymbol{\Psi}_1 = \overline{\mathbf{K}}_b + \lambda\, \bar{\boldsymbol{\Psi}}^T \mathbf{K}_g \boldsymbol{\Psi}_a + \lambda\, \boldsymbol{\Psi}_a^T \mathbf{K}_g \bar{\boldsymbol{\Psi}} + \lambda^2 \boldsymbol{\Psi}_a^T \mathbf{K}_g \boldsymbol{\Psi}_a, \tag{32b}$$

in which

$$\bar{\boldsymbol{\Psi}}^T \mathbf{M}_g \boldsymbol{\Psi}_a = (\boldsymbol{\Phi}_b^d)^T \hat{\mathbf{M}}_c^T \mathbf{A} \text{ with } \mathbf{A} = \mathbf{K}_s^{-1} \hat{\mathbf{M}}_c (\boldsymbol{\Phi}_b^d), \tag{33a}$$

$$\boldsymbol{\Psi}_a^T \mathbf{M}_g \boldsymbol{\Psi}_a = \mathbf{A}^T \mathbf{M}_s \mathbf{A}, \quad \bar{\boldsymbol{\Psi}}^T \mathbf{K}_g \boldsymbol{\Psi}_a = \mathbf{0}, \quad \boldsymbol{\Psi}_a^T \mathbf{K}_g \boldsymbol{\Psi}_a = \bar{\boldsymbol{\Psi}}^T \mathbf{M}_g \boldsymbol{\Psi}_a. \tag{33b}$$

Pre-multiplying $\overline{\mathbf{M}}_b^{-1}$ in Equation (29), we obtain the following relation

$$\bar{\lambda}\, \mathbf{q}_b^d = \mathbf{H}_b \mathbf{q}_b^d \text{ with } \mathbf{H}_b = \overline{\mathbf{M}}_b^{-1} \overline{\mathbf{K}}_b. \tag{34}$$

Substituting the terms in Equation (33) into Equation (32), and using $\bar{\lambda}$ instead of the unknown λ, Equation (32) can be rewritten as

$$\tilde{\mathbf{M}}_b = \overline{\mathbf{M}}_b + \bar{\lambda}\, (\boldsymbol{\Phi}_b^d)^T \hat{\mathbf{M}}_c^T \mathbf{A} + \bar{\lambda} \mathbf{A}^T \hat{\mathbf{M}}_c \boldsymbol{\Phi}_b^d + \bar{\lambda}^2 \mathbf{A}^T \mathbf{M}_s \mathbf{A}, \tag{35a}$$

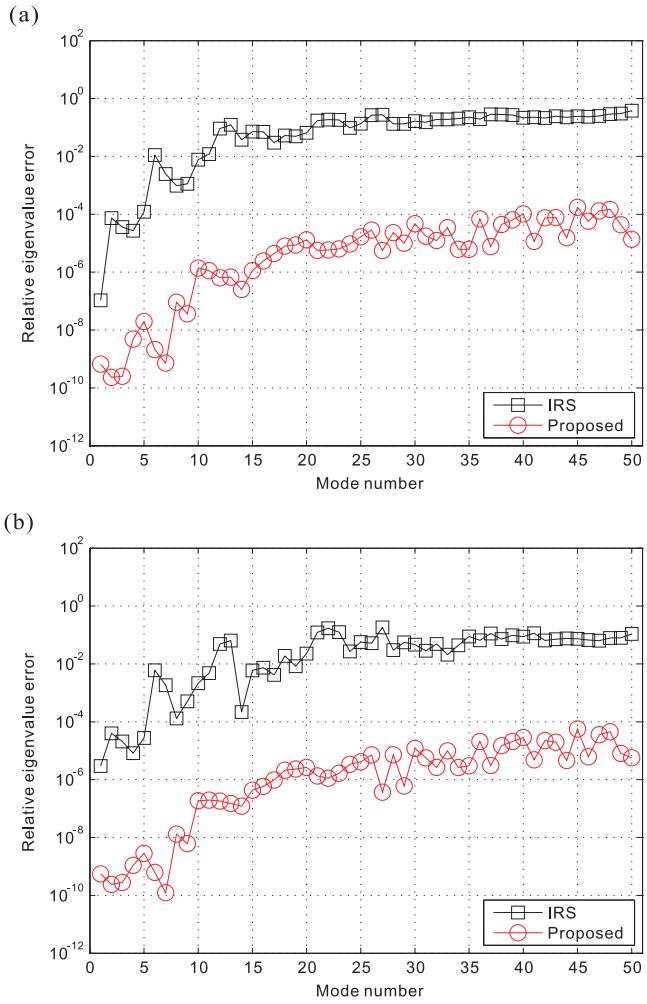

Figure 5. Relative eigenvalue errors by the IRS and proposed methods for the stiffened plate problem: (a) $N_r = 300$ and $\overline{N}_b = 300$ (b) $N_r = 600$ and $\overline{N}_b = 600$.

DOI: 10.1002/nme

$$\tilde{\mathbf{K}}_b = \overline{\mathbf{K}}_b + \bar{\lambda}^2 (\mathbf{\Phi}_b^d)^T \hat{\mathbf{M}}_c^T \mathbf{A}. \tag{35b}$$

Using the relationship $\bar{\lambda}\, \mathbf{q}_b^d = \mathbf{H}_b \mathbf{q}_b^d$ in Equation (34), the reduced matrices in Equation (35) are redefined as

$$\tilde{\mathbf{M}}_b = \overline{\mathbf{M}}_b + (\mathbf{\Phi}_b^d)^T \hat{\mathbf{M}}_c^T \mathbf{A}\, \mathbf{H}_b + \mathbf{H}_b^T \mathbf{A}^T \hat{\mathbf{M}}_c \mathbf{\Phi}_b^d + \mathbf{H}_b^T \mathbf{A}^T \mathbf{M}_s \mathbf{A}\, \mathbf{H}_b, \tag{36a}$$

$$\tilde{\mathbf{K}}_b = \overline{\mathbf{K}}_b + \mathbf{H}_b^T (\mathbf{\Phi}_b^d)^T \hat{\mathbf{M}}_c^T \mathbf{A}\, \mathbf{H}_b, \tag{36b}$$

where the matrix $\mathbf{A}$ can be represented in a submatrix form as

$$\mathbf{A} = \begin{bmatrix} \mathbf{A}_1 \\ \mathbf{A}_2 \\ \vdots \\ \mathbf{A}_n \end{bmatrix} \text{ with } \mathbf{A}_i = (\mathbf{K}_i^s)^{-1} \hat{\mathbf{M}}_i^c (\mathbf{\Phi}_b^d). \tag{37}$$

Substituting $\hat{\mathbf{M}}_c$ in Equation (24) into Equation (36), the reduced matrices of the proposed method are finally obtained in a submatrix form as follows:

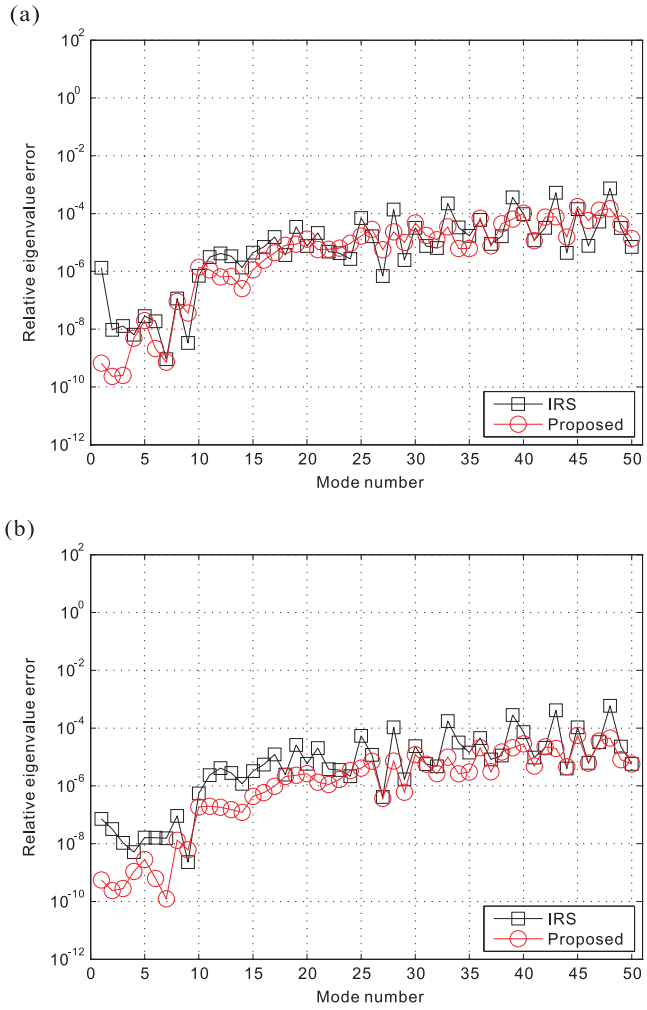

Figure 6. Relative eigenvalue errors by the IRS and proposed methods for the stiffened plate problem: (a) $N_r = 3600$ and $\overline{N}_b = 300$ (b) $N_r = 4200$ and $\overline{N}_b = 600$.

DOI: 10.1002/nme

$$\tilde{\mathbf{M}}_b = \overline{\mathbf{M}}_b + \mathbf{R}_1 + \mathbf{R}_1^T + \mathbf{R}_2, \quad \tilde{\mathbf{K}}_b = \overline{\mathbf{K}}_b + \mathbf{H}_b^T \mathbf{R}_1 \tag{38a}$$

$$\text{with } \mathbf{R}_1 = \sum_{i=1}^{n} (\mathbf{\Phi}_b^d)^T (\hat{\mathbf{M}}_i^c)^T \mathbf{A}_i \mathbf{H}_b, \mathbf{R}_2 = \sum_{i=1}^{n} \mathbf{H}_b^T \mathbf{A}_i^T \mathbf{M}_i \mathbf{A}_i \mathbf{H}_b, \tag{38b}$$

in which $\tilde{\mathbf{M}}_b$ and $\tilde{\mathbf{K}}_b$ are the reduced mass and stiffness matrices of size $\overline{N}_b \times \overline{N}_b$. It is important to note that the reduced matrices are efficiently calculated through multiplications and summations of submatrices without considering the global transformation matrix.

In the proposed method, the eigensolutions are then approximated from the following reduced eigenvalue problem

$$\tilde{\mathbf{K}}_b(\bar{\boldsymbol{\varphi}})_i = \bar{\lambda}_i \tilde{\mathbf{M}}_b (\bar{\boldsymbol{\varphi}})_i \text{ for } i = 1, 2, \ldots, \overline{N}_b, \tag{39}$$

Table IV. Specific computational cost for the stiffened structure problem when $N_r = 3,600$ and $\overline{N}_b = 300$.

Methods	Items	Related Equations	Computation times [sec]	Computation times Ratio [%]
IRS	Transformation procedure	8, 13	5514.97	99.93
	Reduced eigenvalue problem	14	3.74	0.07
	Total	—	5518.71	100.00
Proposed	Algebraic substructuring	16	0.52	0.01
	Calculation of $\hat{\mathbf{M}}_b$ and $\hat{\mathbf{K}}_b$ matrices	25	10.41	0.19
	Eigenvalue problem for the interface boundary	26	16.73	0.30
	Calculation of $\overline{\mathbf{M}}_b$, $\overline{\mathbf{K}}_b$ and $\mathbf{H}_b$ matrices	29, 34	1.12	0.02
	Calculation of $\tilde{\mathbf{M}}_b$ and $\tilde{\mathbf{K}}_b$ matrices	38	12.26	0.22
	Reduced eigenvalue problem	39	0.50	0.01
	Total	—	41.54	0.75

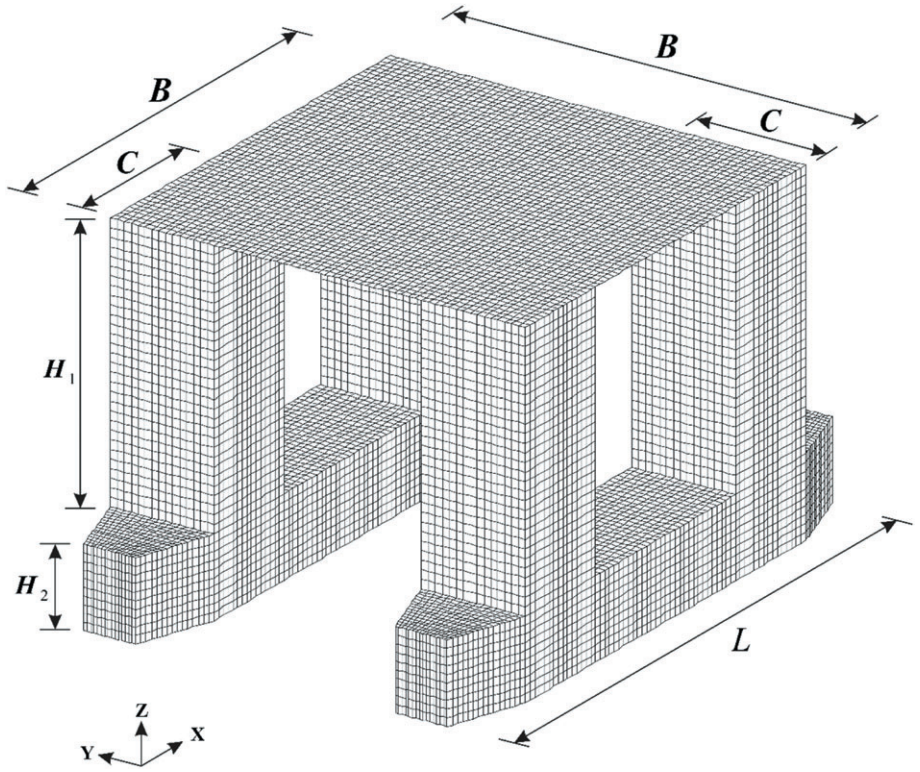

Figure 7. Semi-submersible rig problem (16,800 shell elements, 102,054 DOFs).

DOI: 10.1002/nme

where $\bar{\lambda}_i$ and $(\bar{\varphi})_i$ are the approximated eigenvalues and eigenvectors, respectively.

The approximated global eigenvectors are calculated by

$$(\bar{\varphi}_g)_i = \Psi_1 \bar{\varphi}_i \text{ for } i = 1, 2, \ldots, \overline{N}_b, \tag{40}$$

in which

$$\Psi_1 = \begin{bmatrix} \Psi_1^1 \\ \Psi_2^1 \\ \vdots \\ \Psi_n^1 \\ \Phi_b^d \end{bmatrix} \text{ with } \Psi_i^1 = \Psi_i^c \Phi_b^d + (\mathbf{K}_i^s)^{-1} \hat{\mathbf{M}}_i^c \Phi_b^d \mathbf{H}_b \text{ for } i = 1, 2, \ldots, n. \tag{41}$$

The computational procedure of the algebraic dynamic condensation proposed in this study is summarized in Table I.

4. NUMERICAL EXAMPLES

In this section, the performance of the proposed method is tested considering four practical structural problems frequently handled in the ship and ocean engineering fields – a rectangular plate, a

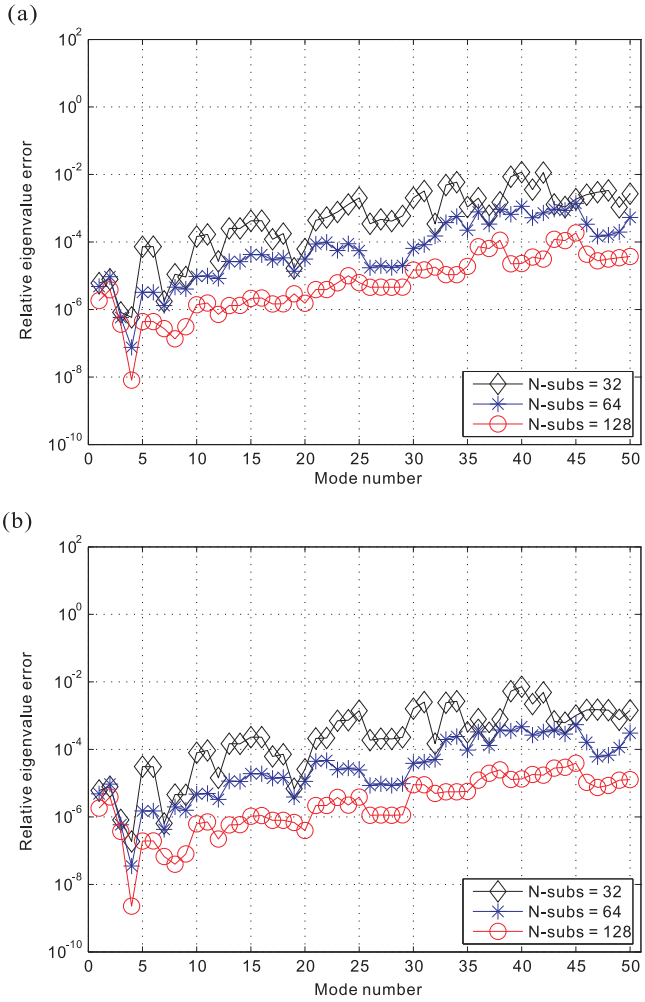

Figure 8. Relative eigenvalue errors by the proposed method for the semi-submersible rig problem, when the number of substructures are 32, 64, and 128: (a) $\overline{N}_b = 300$ (b) $\overline{N}_b = 600$.

DOI: 10.1002/nme

stiffened plate, a semi-submersible rig, and a cargo hold structure. The accuracy and computational efficiency of the proposed method are compared with those of the IRS method.

In the IRS method, the retained DOFs are selected by using the ratio of the diagonal terms of mass and stiffness matrices [4, 6]. In the proposed method, algebraic substructuring is performed using METIS [28], which is an efficient matrix reordering and partitioning software package, and the frequency cut-off method is employed to select the dominant interface normal modes [17].

All the structural problems are modeled using 4-node MITC shell finite elements [35–37], and a free boundary condition is imposed. The material property of a mild steel is used, with Young's modulus E =206 GPa, Poisson's ratio υ =0.3, and density $\rho = 7850\ kg/m^3$. The numerical procedure is implemented in MATLAB and a personal computer (Intel core (TM) i7-3770, 3.40 GHz CPU, 32GB RAM) is used for computation.

To measure the accuracy of reduced models constructed by the IRS and proposed methods, the following relative eigenvalue error is adopted

$$\xi_i = \frac{\overline{\lambda}_i - \lambda_i}{\lambda_i}, \tag{42}$$

in which ξ_i denotes the relative eigenvalue error for the ith mode and the exact global eigenvalue λ_i is obtained from the eigenvalue problem of the global structural FE model in Equation (3).

4.1. Rectangular plate problem

We consider the rectangular plate modeled by a 60 × 36 mesh of 4-node MITC shell finite elements as shown in Figure 2, and the number of DOFs is 11,285. The length L, width B, and thickness h are 20, 12, and 0.025 m, respectively.

Table V. Computational cost for the semi-submersible rig problem when $\overline{N}_b = 300$.

Methods	Number of substructures	Computation times [sec]
IRS	—	N/A
Proposed	32	207.30
	64	101.63
	128	75.89

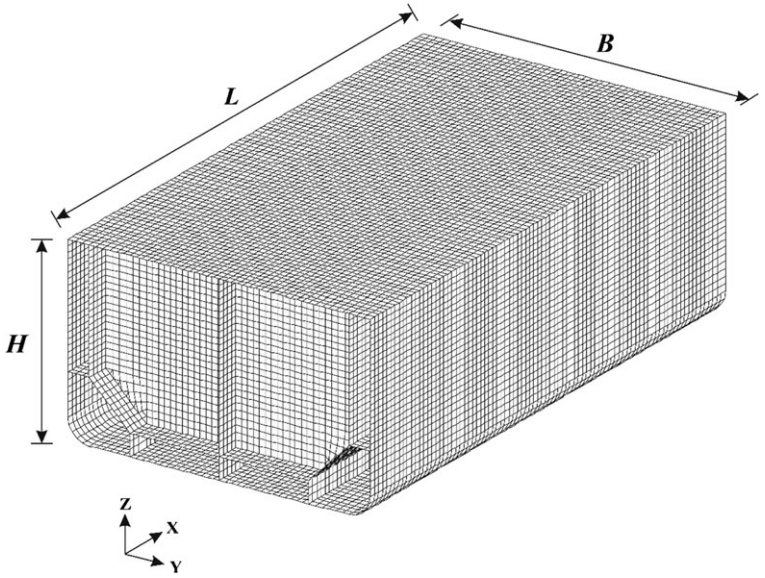

Figure 9. Cargo hold structure problem (26,761 shell elements, 157,368 DOFs).

DOI: 10.1002/nme

The mass and stiffness matrices are partitioned into 16 substructures and interface boundary using algebraic substructuring. Two different sizes of the reduced model are considered: $N_r = \overline{N}_b = 100$ and $N_r = \overline{N}_b = 300$. The performance of the proposed method is compared with that of the IRS method.

Figure 3 presents the relative eigenvalue errors obtained using the IRS and proposed methods in the two numerical cases considered. Table II lists the relative eigenvalue errors when $N_r = \overline{N}_b = 100$. Notice that the proposed method constructs more accurate reduced models than the IRS method. Table III shows the computational cost when $N_r = \overline{N}_b = 100$. Compared with the computation time required for the IRS method, the proposed method only requires 0.96% of the computation time. That is, the proposed method is more than 100 times faster than the IRS method in terms of computation. The results show that the proposed method outperforms the IRS method in both accuracy and computational efficiency.

4.2. *Stiffened plate problem*

As shown in Figure 4, a stiffened plate, an important component of ship structures, is considered. Length L, breadth B, and stiffener spacing S are 26, 6, and 2 m, respectively. The stiffener is composed of a vertical web of height 0.5 m and a flange of breadth 0.2 m, and the thickness h is 0.019 m. The stiffened plate structure is modeled using 8,580 shell finite elements and the number of

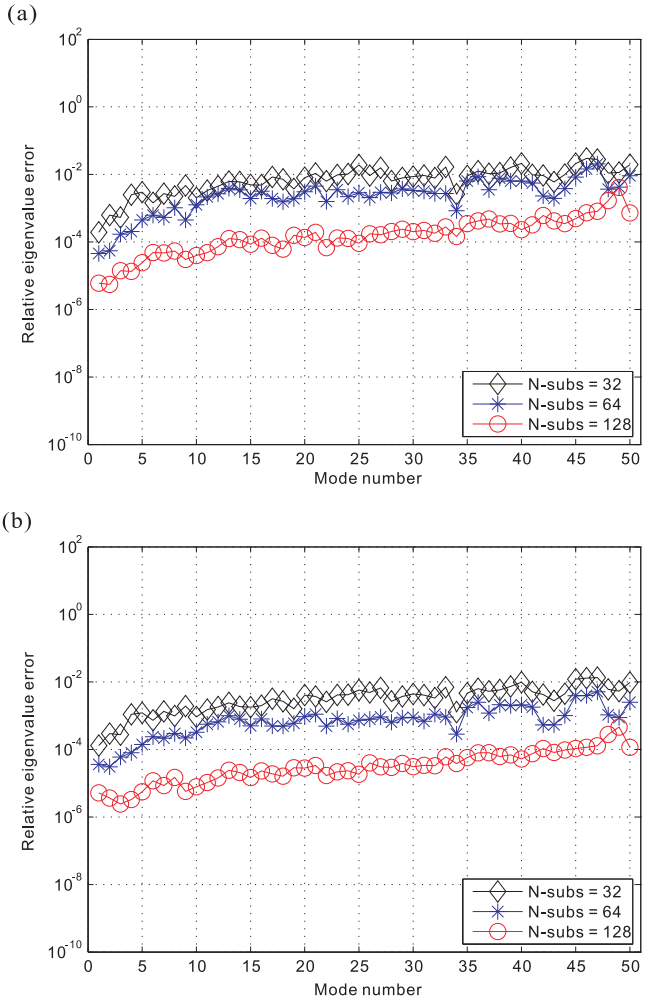

Figure 10. Relative eigenvalue errors by the proposed method for the cargo hold structure problem, when the number of substructures are 32, 64, and 128: (a) $\overline{N}_b = 200$ (b) $\overline{N}_b = 600$.

DOI: 10.1002/nme

DOFs is 52,662. The mass and stiffness matrices are partitioned into 64 substructures and interface boundary using METIS. Figure 5 presents the relative eigenvalue errors obtained using the IRS and proposed methods for two different sizes of the reduced models: $N_r = \overline{N}_b = 300$ and $N_r = \overline{N}_b = 600$. The excellent accuracy of the proposed method is observed in both cases.

We then investigate sizes of the reduced models obtained from the two methods, when the accuracies of the reduced models are similar. As shown in Figure 6, to obtain a similar level of accuracy, the proposed method requires reduced models of sizes, $\overline{N}_b = 300$ and $\overline{N}_b = 600$, and the IRS method requires reduced models of sizes, $N_r = 3,600$ and $N_r = 4,200$. These results show that the pro-

Table VI. Computational cost for the cargo hold structure problem when $\overline{N}_b = 200$.

Methods	Number of substructures	Computation times [sec]
IRS	—	N/A
Proposed	32	496.30
	64	221.72
	128	133.01

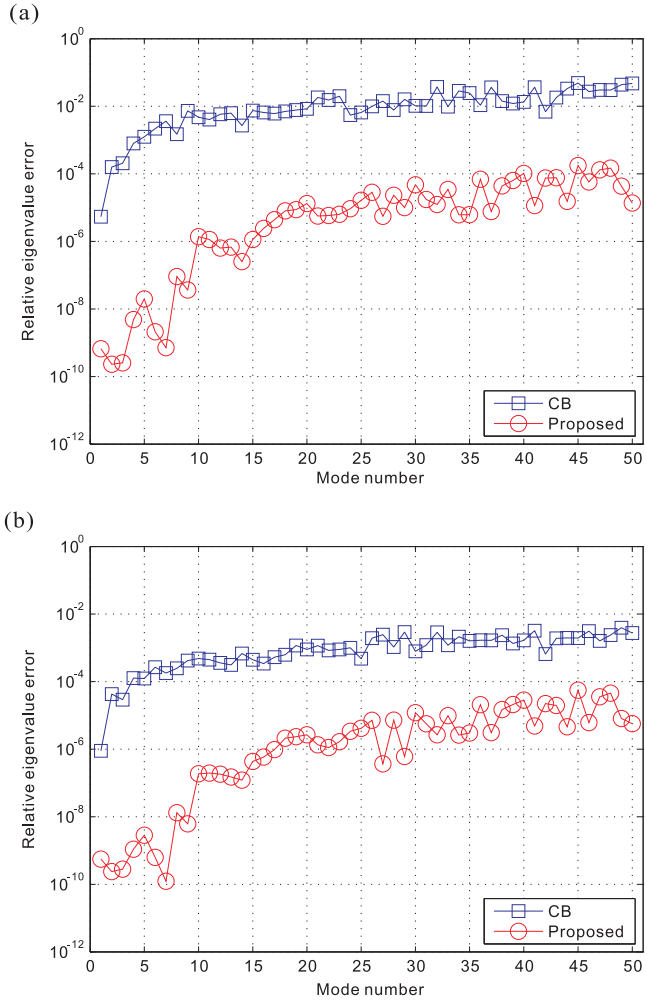

Figure 11. Relative eigenvalue errors by the CB and proposed methods for the stiffened plate problem: (a) $N_p = 3,582$(CB) and $\overline{N}_b = 300$(proposed), (b) $N_p = 3,722$(CB) and $\overline{N}_b = 600$(proposed).

DOI: 10.1002/nme

posed method can provide much smaller reduced models for a desired accuracy. The computational cost required is presented in Table IV when $\overline{N}_b = 300$ and $N_r = 3,600$.

4.3. Semi-submersible rig problem

A semi-submersible rig structure shown in Figure 7 is considered. The corresponding breadth B, column width C, and heights H_1 and H_2 are 80, 20, 50, and 15 m, respectively. The length L and thickness h of the structure are 110 and 0.018 m, respectively. The structure was modeled using 16,800 shell finite elements and 102,054 DOFs. In this FE model, the IRS method fails to construct any size of reduced models because of the large size of computer memory required for storing almost fully populated matrices, $\mathbf{T}_G$ and $\mathbf{T}_a$.

Using METIS, the global mass and stiffness matrices of the FE model are partitioned into 32, 64, and 128 substructures. We construct two different sizes of the reduced model: $\overline{N}_b = 300$ and $\overline{N}_b = 600$. We then investigate the effect of the number of substructures on the performance of the proposed method. Figure 8 and Table V show that, as the number of the substructures increases, both accuracy and computational efficiency improve; a particularly interesting feature of the proposed method.

4.4. Cargo hold structure problem

Finally, we consider a cargo hold structure of an oil carrier as shown in Figure 9. The height H, breadth B, length L, and thickness h of the carrier are 30, 50, 87, and 0.025 m, respectively. We use 26,761 shell finite elements and 26,228 nodes for finite element modeling. The number of DOFs is 157,368. In this case, the IRS method also does not work.

The global mass and stiffness matrices are partitioned into 32, 64, and 128 substructures. Two numerical cases are considered: $\overline{N}_b = 200$ and $\overline{N}_b = 600$. Figure 10 and Table VI present the accuracy and computational efficiency of the proposed method, respectively. As the number of the substructures increases, the performance of the proposed method also grows.

5. COMPARISON WITH THE CRAIG BAMPTON METHOD

In this section, we compare the accuracy and computational efficiency of the proposed method with those of the CB method, a well-known CMS method widely used in structural dynamics.

In the CB method, the reduced mass and stiffness matrices are calculated by

$$\overline{\mathbf{M}} = \bar{\mathbf{T}}_{CB}^T \mathbf{M}_g \bar{\mathbf{T}}_{CB}, \quad \overline{\mathbf{K}} = \bar{\mathbf{T}}_{CB}^T \mathbf{K}_g \bar{\mathbf{T}}_{CB} \text{ with } \bar{\mathbf{T}}_{CB} = [\, \mathbf{\Phi}_d \;\; \mathbf{\Psi} \,], \tag{43}$$

where $\bar{\mathbf{T}}_{CB}$ is the transformation matrix of the CB method, which is constructed using the dominant fixed-interface normal modes $\mathbf{\Phi}_d$ obtained from the substructural eigenvalue problems [17, 23] and the interface constraint modes $\mathbf{\Psi}$. The detailed formulation of the CB method is shown in References [17, 23].

The major differences between the CB and proposed methods comes from how to accomplish the substructuring, and whether the substructural eigenvalue problems are solved or not. With the CB method, the substructuring is accomplished manually using the physical domain-based partitioning considering the geometrical characteristics of the global structure. This means that it is difficult to construct a large number of substructures using this method.

Let us consider the case that a large size FE model (over 10^5 DOFs) is handled using the CB method. When the number of substructures used is small, each substructure contains relatively large DOFs. Then, the computational costs for calculating the dominant fixed-interface normal modes $\mathbf{\Phi}_d$ and the interface constraint modes $\mathbf{\Psi}$ becomes expensive. Even if the global structure is partitioned into many substructures, it induces a considerably larger interface boundary; thus the size of the reduced system also becomes large. That is, in any case, the CB method has limitations for dealing with large FE models.

On the other hand, with the proposed method, the substructuring procedure is automatic from the aspect of algebraic perspective, and it provides the potential to make hundreds of the substructures

DOI: 10.1002/nme

without considering a physical domain. Therefore, we can handle very small submatrices and the interface constraint modes $\boldsymbol{\Psi}$ that require large computational cost in the CB method, can be calculated very efficiently. Furthermore, using the proposed method, there is no need to calculate the dominant fixed-interface normal modes $\boldsymbol{\Phi}_d$. This feature is a benefit of the proposed method that saves computational costs compared with CMS methods.

To compare the performances of the CB and proposed methods, the stiffened plate problem in Figure 4 is considered again. We reuse the numerical results described in Figure 5 and Table VI for the proposed method. For the CB method, the stiffened plate is partitioned evenly into 18 substructures, and the size of the interface boundary N_b is 3,522. The detailed partitioning information is shown in Reference [23]. For two numerical cases, we use 60 and 200 dominant substructural modes ($N_d = 60$ and $N_d = 200$) and the reduced size of the matrices, N_p (where $N_p = N_d + N_b$), are 3,582 and 3,722, respectively. Figure 11 shows the relative eigenvalue errors obtained by the CB and proposed methods, and Table VII lists the relative eigenvalue errors for the 1st–25th global modes corresponding to Figure 11(a). We observe that the proposed method gives more accurate reduced models than those obtained by the CB method, even though using reduced models that are much smaller. Table VIII shows the computational cost. Compared with the computation time required for

Table VII. Relative eigenvalue errors for the stiffened plate problem in Figure 11(a).

Mode number	CB	Proposed
1	5.39755E-06	5.27029E-10
2	1.59490E-04	2.30534E-10
3	2.06890E-04	2.45733E-10
4	7.96874E-04	4.85340E-09
5	1.24680E-03	1.97862E-08
6	2.18312E-03	2.10973E-09
7	3.62139E-03	7.19681E-10
8	1.49353E-03	9.13311E-08
9	7.30045E-03	3.63130E-08
10	4.73748E-03	1.38734E-06
11	4.03604E-03	1.13632E-06
12	5.81648E-03	6.35017E-07
13	6.26525E-03	6.75291E-07
14	2.68507E-03	2.50865E-07
15	7.47668E-03	1.13370E-06
16	6.58250E-03	2.42809E-06
17	6.09378E-03	4.40237E-06
18	7.02676E-03	7.97968E-06
19	7.74041E-03	8.72474E-06
20	8.42764E-03	1.31524E-05
21	1.82465E-02	5.62026E-06
22	1.53537E-02	5.85527E-06
23	1.99614E-02	6.37930E-06
24	5.50344E-03	9.32504E-06
25	6.53516E-03	1.65506E-05

Table VIII. Computational cost for the stiffened structure problem in Figure 11(a) (The sizes of the reduced models considered: $N_p = 3,582$ and $\overline{N}_b = 300$ for the CB and proposed methods, respectively).

Methods	Items	Computation times [sec]	Computation times Ratio [%]
CB	Calculation of the dominant fixed interface normal modes $\boldsymbol{\Phi}_d$	23.03	13.94
	Calculation of the interface constraint modes $\boldsymbol{\Psi}$	124.43	75.30
	Transformation procedure	17.78	10.76
	Total	165.24	100.00
Proposed		41.54	25.14

DOI: 10.1002/nme

the CB method, the proposed method requires only 25.14 % of the computation time. Therefore, we can say that the proposed method is more competitive than the CB method regarding the aspects of accuracy and efficiency.

6. CONCLUSIONS

In this study, the algebraic dynamic condensation method is proposed. Employing algebraic substructuring, the global mass and stiffness matrices are automatically partitioned into many small submatrices, and these submatrices are designated as the substructures and interface boundary. The substructural stiffness is condensed into the interface boundary, and then the interface boundary is reduced considering only the dominant interface normal modes. Finally, the reduced model is constructed by condensing the substructural inertial effects into the reduced interface boundary. The formulation was derived at a submatrix level to avoid expensive global matrix operations and matrix populations. We investigated the excellent accuracy and computational efficiency of the proposed method through various practical structural problems. The proposed method handled relatively large FE models, for which the IRS method failed to work, and showed more competitive performance than the CB method.

In future work, to solve FE models with more than several millions of DOFs, it would be valuable to develop a more efficient algebraic dynamic condensation method employing the multilevel algebraic substructuring. Based on the proposed method, an effective iterative scheme could also be developed. A mathematical investigation of such a method would significantly further the understanding of the characteristics of the proposed method.

ACKNOWLEDGEMENTS

This research was supported by Basic Science Research Program through the National Research Foundation of Korea(NRF) funded by the Ministry of Science, ICT Future Planning(No. 2014R1A1A1A05007219), and a grant (MPSS-CG-2016-04) through the Disaster and Safety Management Institute funded by Ministry of Public Safety and Security of Korean government.

REFERENCES

1. Guyan R. Reduction of stiffness and mass matrices. *AIAA Journal* 1965; **3**(2):380.
2. Irons BM. Eigenvalue economisers in vibration problems. *Journal of the Royal Aeronautical Society* 1963; **67**:562.
3. Kidder RL. Reduction of structural frequency equations. *AIAA Journal* 1973; **11**(6):892–892.
4. Henshell RD, Ong JH. Automatic masters from eigenvalues economization. *Earthquake Engineering and Structural Dynamics* 1975; **3**:375–383.
5. Paz M. Dynamic condensation method. *AIAA Journal* 1984; **22**(5):724–727.
6. Ong JH. Improved automatic masters for eigenvalues economization. *Finite Elements in Analysis and Design* 1987; **3**(2):149–160.
7. O'Callanhan J. A procedure for an improved reduced system (IRS) Model. *Proceeding the 7th International Modal Analysis Conference*, Bethel, CT, 1989; 17–12.
8. Mottershead JE, Friswell MI. Model updating in structural dynamics: a survey. *Journal of Sound and Vibration* 1993; **2**:347–375.
9. Suarez LE. Dynamic condensation method for structural eigenvalue analysis. *AIAA Journal* 1992; **30**(4):1046–1054.
10. Friswell MI, Garvey SD, Penny JET. Model reduction using dynamic and iterated IRS techniques. *Journal of Sound and Vibration* 1995; **186**(2):311–323.
11. Xia Y, Lin R. A new iterative order reduction (IOR) method for eigensolutions of large structures. *International Journal for Numerical Methods in Engineering* 2004; **59**:153–172.
12. Bouhaddi N, Fillod R. Substructuring using a linearized dynamic condensation method. *Computers & Structures* 1992; **45**(4):679–683.
13. Bouhaddi N, Fillod R. A method for selecting master DOF in dynamic substructuring using the Guyan condensation method. *Computers & Structures* 1992; **45**(5):941–946.
14. Bouhaddi N, Fillod R. Substructuring by a two level dynamic condensation method. *Computers & Structures* 1996; **60**(3):403–409.
15. Hughes TJR. *The Finite Element Method: Linear Static and Dynamic Finite Element Analysis*. Dover: Mineola, NY, USA, 2000.
16. Hurty W. Dynamic analysis of structural systems using component modes. *AIAA Journal* 1965; **3**(4):678–685.
17. Craig RR, Bampton BCC. Coupling of substructures for dynamic analysis. *AIAA Journal* 1968; **6**(7):1313–1319.

DOI: 10.1002/nme

18. MacNeal RH. Hybrid method of component mode synthesis. *Computers & Structures* 1971; **1**(4):581–601.
19. Benfield WA, Hruda RF. Vibration analysis of structures by component mode substitution. *AIAA Journal* 1971; **9**:1255–1261.
20. Kuhar EJ, Stahle CV. Dynamic transformation method for modal synthesis. *AIAA Journal* 1974; **12**(5):672–678.
21. Rubin S. Improved component-mode representation for structural dynamic analysis. *AIAA Journal* 1975; **13**(8): 995–1006.
22. Bourquin F. Component mode synthesis eigenvalues of second order operators: discretization and algorithm. *Math Model Numer Analysis* 1992; **26**(3):385–423.
23. Boo SH, Kim JG, Lee PS. A simplified error estimator for the Craig–Bampton method and its application to error control. *Computers & Structures* 2016; **164**:53–62.
24. Kim H, Cho M. Improvement of reduction method combined with sub-domain scheme in large-scale problem. *International Journal for Numerical Methods in Engineering* 2007; **70**:206–251.
25. Choi D, Kim H, Cho M. Iterative method for dynamic condensation combined with substructuring scheme. *Journal of Sound and Vibration* 2008; **317**(1):199–218.
26. George A. Nested dissection of a rectangular finite element mesh. *SIAM Journal on Numerical Analysis* 1973; **10**(2):345–363.
27. Hendrickson B, Rothberg E. Effective sparse matrix ordering: just around the bend. *Proceedings of Eighth SIAM Conference on Parallel Processing for Scientific Computing*, Minneapolis, Minnesota, 1997.
28. Karypis G. METIS v4, A software package for partitioning unstructured graphs, partitioning meshes, and computing fill-reducing orderings of sparse matrices. *Technical Report ,* University of Minnesota: Minneapolis, MN, 1998.
29. Yang C, Gao W, Bai Z, Li XS, Lee LQ, Husbands P, NG E. An algebraic substructuring method for large-scale eigenvalue calculation. *SIAM Journal on Scientific Computing* 2005; **27**(3):873–892.
30. Kaplan MF. Implementation of automated multi-level substructuring for frequency response analysis of structures. *Ph.D. thesis*, Department of Aerospace Engineering & Engineering Mechanics, University of Texas at Austin, Austin, TX, 2001.
31. Bennighof JK, Lehoucq RB. An automated multilevel substructuring method for eigenspace computation in linear elastodynamics. *SIAM Journal on Scientific Computing* 2004; **25**(6):2084–2106.
32. Kim JG, Boo SH, Lee PS. An enhanced AMLS method and its performance. *Computer Methods in Applied Mechanics and Engineering* 2015; **287**:90–111.
33. Boo SH, Kim JG, Lee PS. Error estimation method for automated multi-level substructuring method. *International Journal for Numerical Methods in Engineering* 2016; **106**:927–950.
34. Baek SM. Study on the multi-level substructuring scheme and system condensation for the large-scaled structural dynamic analysis. *Ph.D. thesis*, Department of Mechanical and Aerospace Engineering, Seoul National University, 2012.
35. Dvorkin EN, Bathe KJ. A continuum mechanics based four-node shell element for general nonlinear analysis. *Engineering Computations* 1984; **1**(1):77–88.
36. Lee PS, Bathe KJ. Development of MITC isotropic triangular shell finite elements. *Computers & Structures* 2004; **82**(11-12):945–962.
37. Lee YG, Lee PS, Bathe KJ. The MITC3+ shell finite element and its performance. *Computers & Structures* 2014; **138**:12–23.

DOI: 10.1002/nme